


FULL ARTICLE

Peri-tumoural stroma collagen organization of invasive ductal carcinoma assessed by polarized light microscopy differs between OncotypeDX risk group

Blake Jones¹  | Georgia Thomas¹ | Jillian Sprenger¹ | Sharon Nofech-Mozes² | Mohammadali Khorasani³ | Alex Vitkin^{1,4,5*}

¹Department of Medical Biophysics, University of Toronto, Toronto, Canada

²Department of Laboratory Medicine and Pathobiology, University of Toronto, Toronto, Canada

³Department of Surgery, University of British Columbia, Victoria, Canada

⁴Division of Biophysics and Bioimaging, Princess Margaret Cancer Centre, Toronto, Canada

⁵Department of Radiation Oncology, University of Toronto, Toronto, Canada

*Correspondence

Alex Vitkin, 101 College Street, M5G1L7 Toronto, Canada.

Email: alex.vitkin@rmp.uhn.ca

Funding information

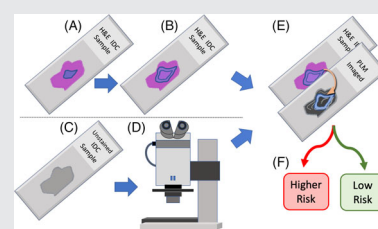
Canadian Institutes of Health Research, Grant/Award Number: PJT-156110; Natural Sciences and Engineering Research Council of Canada, Grant/Award Number: 410009540

Abstract

A commercially available genomic test, OncotypeDX has emerged as a useful post-surgical treatment guide for early stage breast cancer. Despite widespread clinical adoption, there remain logistical issues with its implementation. Collagenous stromal architecture has been shown to hold prognostic value that may complement OncotypeDX. Polarimetric analysis of breast cancer surgical samples allows for the quantification of collagenous stroma abundance and organization. We examine intratumoural collagen abundance and alignment along the tumor-host interface for 45 human samples of invasive ductal carcinoma categorized as low or higher risk by OncotypeDX. Furthermore, we probe the separatory power of collagen alignment patterns to classify unlabeled samples as low or higher OncotypeDX risk group using a linear discriminant (LD) model. No significant difference in mean collagen abundance was found between the two risk groups. However, collagen alignment along the tumor boundary was found to be significantly lower in higher risk samples. The LD model achieved a 71% total accuracy and 81% sensitivity to higher risk samples. Prognostic information extracted from the stromal morphology has potential to complement OncotypeDX as an easy-to-implement prescreening methodology.

KEYWORDS

breast cancer, collagen, microscopy, OncotypeDX, polarized light, prognostication, tumor microenvironment



1 | INTRODUCTION

Despite extensive research and clinical efforts, breast cancer remains a challenging public health issue and the largest cause of oncologic mortality among women.^[1] Its

therapeutic management is complicated by the heterogeneous nature of tumor behaviors and patient outcomes within its subclasses.^[2] Tailoring treatment regimens in light of this diversity has long been the goal of personalized medicine in oncology. However, in order to realize the full potential of individualized therapy, there is a

Mohammadali Khorasani and Alex Vitkin are senior coauthors

need to develop robust prognostic tools that are accurate, affordable and logistically implementable.

One successful approach in the context of breast cancer is a genomic test known as OncotypeDX. This test, performed on surgical specimens, assesses the expression levels of 21 genes (16 cancer-related and 5 reference) to predict the likelihood of cancer recurrence within a given number of years (5 years for node-positive cases or 10 years for node-negative).^[3, 4] While validation is ongoing for other subgroups (eg, HER-2 positive tumors), currently OncotypeDX serves as a prognostic and predictive tool in hormone receptor positive and HER-2 negative invasive breast cancer capable of guiding clinical decisions regarding the benefit of adjuvant systemic chemotherapy.^[5] The output of the test is a numerical Risk Recurrence Score on a scale of 1 to 100, subcategorized into low, intermediate and high-risk tumors.^[5]

However, despite the adoption of OncotypeDX into the standard of care in certain settings, there remain some unaddressed challenges. First, as mentioned above, the test is typically limited to invasive, hormone receptor positive, HER-2 negative tumors. These criteria evidently exclude a significant subgroup of breast cancer patients. In addition, the test is very expensive at approximately \$4000 USD per test.^[6] This limits its incorporation into some clinical workflows, particularly in developing economies or among populations lacking private insurance.^[7] In addition, there remains a degree of uncertainty as to the test's accuracy in cases of highly heterogeneous tumor in which gene expression may be spatially variable.^[8, 9]

As a result of these limitations, there is a need for the development of additional, complementary prognostic markers for breast cancer. Optical approaches, though perhaps less specific in tumor classification than the detailed expression information obtained by genomic approaches, have potential as a complementary tool. These methods are particularly useful because of their high-resolution visualization of various tissue constituents. In addition, relatively large regions of tissue can be assessed, addressing spatial heterogeneity concerns, and often with high contrast and in near real time.^[10] Importantly, optical techniques can be used to assess characteristics of the tumor microenvironment (TME) which have shown potential as a source of prognostic information.^[11, 12] Indeed, solid tumors do not exist in isolation: it has long been known that the tissues within the tumor mass itself and those surrounding the tumor play an essential role in maintaining its viability, growth characteristics and metastatic spread potential.^[12, 13]

One compartment of the TME that has shown promise in terms of prognostication is the collagenous stroma. Collagen is a fibrous connective tissue that provides structural support to its surroundings. Higher relative

abundance of intratumoural collagen, known as tumour-stroma ratio (TSR), has been associated with worse patient outcomes in breast and other cancers.^[14–19] In addition to intratumoural abundance, the morphology (or organization) of the collagen around the tumor (in the peri-tumoural region referred to as the leading edge), has also been considered as a biomarker for disease progression and/or prognosis.^[11, 20–23] In order to grow, tumors must invade the surrounding healthy tissue; this invasion is at least in part facilitated by the degradation of the extracellular matrix (ECM) in this boundary region. Therefore, it has been hypothesized that reorganization (induced disorganization), of the collagen in the leading edge of the tumor is indicative of disease progression and is a precursor for further tumor invasion.^[20, 24]

Previous efforts by our group have demonstrated the potential of a novel form of polarimetric imaging to analyze the organization of collagenous stroma in breast cancer samples.^[25, 26] For example, we have used this polarized light imaging approach to develop a quantitative stromal architecture signature (SAS) score capable of differentiating myxoid from sclerotic stroma within the TME. Herein we extend this approach to examine the correlation of polarimetrically derived collagen morphology metrics with OncotypeDX risk groups. The two metrics, one related to the TSR (abundance of collagenous stroma) within the tumor, and the other related to the collagen morphology (alignment) in the leading edge regions, were used to probe the differences between samples of different OncotypeDX risk scores.

The purpose of this research is to address the issues associated with OncotypeDX previously outlined above: its high (and frequently prohibitive) cost, and the spatial heterogeneity of breast tumors. The polarimetric technique for examining the stroma is inexpensive, rapid and can be performed locally on site without the necessity of sending samples for testing and awaiting results; further, neither technical expertise nor significant maintenance by clinical staff are needed. The methodology is also capable of whole slide analysis, potentially capturing more information than is available with a simple biopsy. Using the polarimetry method to separate between low and higher risk groups may eventually provide a robust method for prescreening that can streamline patients and prioritize the genomic testing for those who would stand to benefit (ie, those at higher risk). Apart from increasing our knowledge of the dynamics between breast tumors and their surrounding environment, demonstrating a correlation between stromal morphology changes and a clinically relevant recurrence likelihood score could serve as an impetus for the development of further quantitative polarimetric tools for prognosis and study of the TME.

2 | EXPERIMENTAL

2.1 | Ethics

Institutional ethics approval was obtained from participating hospital institutions (University Health Network and Sunnybrook Hospital, both in Toronto, Canada). The need for patients' consent to examine the breast cancer histopathology samples was waived by the ethics board due to the retrospective nature of the study and complete anonymization of personal health information.

2.2 | Samples

This study used 45 human surgical samples of invasive ductal carcinoma (IDC) prior to any chemo- or radiation-therapy. There were 27 samples from the OncotypeDX low-risk group, 14 in the intermediate group, and four in the high-risk group. For the analysis described below, intermediate and high were pooled together and referred to as the higher risk group; this allowed us to test our method's differentiation ability between the low-risk patients vs all others (most relevant group separation based on clinical considerations^[3]). Samples were formalin-fixed, paraffin embedded, unstained and 4.5 μm thick. To avoid polarization imaging artifacts, the unstained samples were chemically dewaxed^[27] and were then ready for polarimetric imaging, with no further processing nor the use of a coverslip. Tissue slides adjacent to the polarimetrically imaged ones were H&E stained and imaged at $\times 20$ on an Aperio ScanScope CS (Leica Biosystems, Germany) for the pathologist's assessment of the regions of interest (ROIs).

2.3 | ROIs-selection

The selection of suitable ROIs for our analysis was intended to quantify (1) intratumoural collagen abundance, and (2) collagen alignment/orientation in the leading edge of peri-tumoural regions (Figure 1). Relative collagen abundance was hypothesized to be higher in the higher risk OncotypeDx group, as previous work has correlated an increase in collagenous stroma abundance (quantified via TSR) with worse patient outcomes in breast cancer.^[14–19] To enable (1), tumors were contoured using the H&E stained adjacent slides that were then computationally coregistered to the polarimetric images using affine transforms and MATLAB's (Mathworks, Massachusetts) image processing toolbox. In an attempt to account for the intrasample heterogeneity, multiple tumor regions from within each slide were selected. For example,

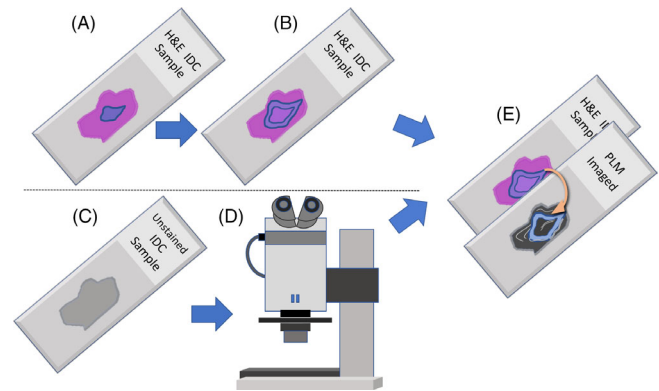


FIGURE 1 Sample annotation and imaging process. A, H&E stained IDC surgical samples were imaged at $\times 20$ and tumor ROIs were contoured (purple region). B, Leading edge region was calculated by an expansion of the tumor contour followed by removal of the original contour (purple band region). C, D, Adjacent unstained slides were imaged using the polarized light microscopy system. E, H&E image and associated annotations are computationally coregistered with the polarized light microscopy image and the corresponding ROIs were transferred (yellow arrow). White features on black background pictorially represent collagen fibers on the polarimetric image. IDC, invasive ductal carcinoma; ROIs, regions of interest

when a sample contained multiple tumor morphologies (eg, ill-defined tumor edge vs well-circumscribed dense nests of cancer cells), both were used in ROI selection.

The purpose of selecting (2), the leading edge ROIs, was that collagen reorganization and remodeling facilitating tumor invasion and growth has been shown to occur primarily along the boundaries of tumors in breast and other cancers.^[21–23, 28, 29] By examining the collagenous alignment within the site of this reorganization, we again aim to identify differences between samples with low and higher OncotypeDX risk recurrence scores. Once regions of tumor were contoured, leading edge regions were obtained by the computational expansion of the contours. This was done by dilating the contours with a circular structural element with a radius of 150 μm . After the expansion, the original tumor contour was removed from the dilated region, leaving the leading edge “strip” 150 μm wide (Figure 1B). Different dilation thicknesses were explored but 150 μm was selected as the compromise between increasing the total area under consideration vs limiting the influence of collagen that was distant from, and thus likely less representative of tumor interaction with the host stroma.

2.4 | Polarimetric imaging

Imaging was done using the previously described polarimetric microscopy setup and methodology.^[25, 26] Polarized

light microscopy (PLM) is a well-established approach for enhancing the contrast of birefringent materials such as collagen. An AxioZoom V16 microscope (Zeiss, Germany) was fitted with two linear polarizers (Thorlabs, LPVISE100-A) and controlled with motorized rotation mounts (PRM1.MZ8, Thorlabs, New Jersey). The IDC slides were placed between the polarizers, which were kept at 90° relative to each other (crossed polarizer orientation). The crossed polarizer pair was then rotated through 90° in 5° increments; this important process facilitates the removal of image contrast variations that depend on polarizer orientation relative to breast tissue's birefringent (collagen) structures, enabling high-contrast visualization of the latter. After each rotation, an image of the sample was taken. The resultant series of images is then analyzed, and the relevant metrics were extracted (see below). Further details of this implementation of the PLM have been recently described.^[25, 26]

2.5 | Image analysis and quantitative metrics extraction

Two metrics, namely abundance and alignment, were extracted from the polarimetric images for each sample. Both were previously used by our group to assess collagenous stroma in breast cancer,^[25, 26] and each examines a distinct feature.

2.5.1 | Abundance metric

The first is related to the amount of birefringent connective tissue (likely collagen) within the tumor. It is the fraction of the total analyzed region that contains birefringent tissue (Figure 2B). Its numerical scale ranges from 0 to 1 (where 1 would indicate an area entirely filled with birefringent tissue). A pixel from the stack of angular measurements that represents a birefringent tissue has an intensity pattern given by:

$$\text{Intensity} \propto \sin^2(2\tau), \quad (1)$$

where τ represents the angle between the optical axis of the structure and the analyzer polarization direction. Therefore, whether a particular pixel represents a birefringent structure can be assessed with a “goodness-of-fit” comparison between the observed intensity pattern of the angular images and Equation (1). Once calculated, this metric can be used to segment the collagenous stroma from other biological compartments, and the collagen density can be calculated. Due to recent evidence linking increased collagen content in tumors to poorer patient outcomes^[14–19] the

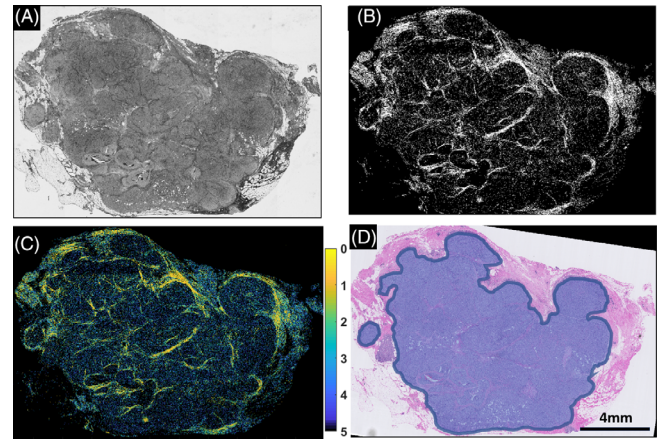


FIGURE 2 Representative images of an IDC sample all taken at $\times 20$. A, White light image of the unstained tissue sample. B, Polarimetrically derived image of the birefringent tissue (collagen), used to calculate the collagen abundance in tumor ROIs. This is a binarized image where “on” pixels (white) indicate the presence of a birefringent tissue regions with many “on” pixels have a high collagen abundance metric. C, Polarimetric alignment image, used to calculate the alignment of collagen in the leading edge ROIs. Low values (yellow) indicate a higher degree of alignment between neighboring structures. D, H&E stained adjacent sample with the tumor contour shown in blue and the leading edge region as the darker band surrounding the contour. IDC, invasive ductal carcinoma; ROIs, regions of interest

abundance metric was calculated for the ROIs within the tumor contours (Figure 1A), yielding a single number for each of the 45 samples. This tested whether the polarimetrically quantified amount of intratumoural collagen differs between OncotypeDX risk groups.

2.5.2 | Alignment metric

The second calculated metric (Figure 2C) describes the relative orientation of all the birefringent structures in a given FOV. The direction of optical axis for a birefringent structure is related to the value of τ at which the measured transmitted intensity is maximal. Once the optical axis direction has been computed, the alignment metric, related to the mean angular difference between collagenous structures in a $30 \times 30 \mu\text{m}$ sliding window, is calculated by:

$$\text{MAD} \equiv \frac{\sum_{i=1}^{n-1} \sum_{j=i+1}^n |B(i) - B(j)|}{\frac{n(n-1)}{2}}, \quad (2)$$

where n is the number of pixels in the sliding window and $B(x)$ is the birefringence orientation at pixel x . Here, x indicates the linear index of a pixel in the sliding

window. As a result of the $\tau = 5^\circ$ increments used in the imaging protocol, the alignment metric can range from 0 (perfect alignment of all the collagen in the window) to 5 (maximal difference, random orientation). The metric was calculated in the leading edge ROIs. Contrasted with the abundance metric, which yields one number per region, a distribution of alignment scores is generated for the leading edge. Therefore, every sample yields a histogram of collagen alignment along the tumor edge.

2.6 | Statistical methods

First, the abundance metric was calculated for each sample's intratumoural collagen. The values from the low and higher risk groups were then compared using a two-sample nonparametric Kolmogorov–Smirnov (KS) test. Next, the leading edge peri-tumoural collagen alignment distributions were analyzed in two ways: using single-number KS comparisons of averaged mean alignments (similar to the abundance analysis above), and then more extensively accounting for their full spectrum. For the latter, we calculated the cumulative density functions (CDFs) for the alignment of collagen in the leading edge for each sample. CDFs from the same OncotypeDX risk group were then combined, allowing for the investigation of differences in the overall distributions of alignment, instead of just comparing means.

Finally, after assessing the differences in the leading edge collagen alignment for low and higher risk groups, and thus generating population distributions of this metric for the two groups, we addressed the more difficult problem of predicting a tumor's OncotypeDX risk group based on the collagen alignment. To accomplish this, we trained a linear discriminant (LD) model using the information-rich alignment CDF formalism. However, incorporation of the entire CDF into the feature-space for a model would result in a predictive feature dimensionality that was prohibitively high given the modest number of samples ($n = 45$). We thus calculated the root mean squared error (RMSE) between every sample's CDF and the combined "population" CDFs for the low and higher risk groups. Although this does lose some of the information contained in the histograms, using the RMSE enabled us to compare the similarity of the collagen alignment distributions while limiting our predictor variable dimensionality from 60 (the number of bins used in the CDF histograms) to 2 (the RMSE between the sample and the low and higher risk groups). As we are dealing with a limited dataset of unique patients, keeping a low-predictor dimension was an important part of mitigating model over-fitting.

The two RMSEs were calculated for each sample and then served as predictor variables for training an LD

model. To offset the effects of the differences in population size for the two groups (27 and 18, respectively) and to maximize the sensitivity to higher risk samples, the cost function used in training the LD model weighed the misclassifications of high-risk samples $\times 3$ greater than misclassifications of low-risk samples. The $\times 3$ weight was chosen because the low and higher risk population sizes differed by a factor of 1.5, which was a starting point for the cost function alteration; further, misclassification of a higher risk tumor as a low risk has significant clinical consequences. The resultant $\times 3$ differential weighting in the cost function penalty thus served as the compromise between total accuracy and the false negative rate. To further prevent over-fitting and to evaluate its performance, we subjected the model to 3-fold cross-validation. Briefly, this entailed dividing the data into three groups of equal size and with equal proportion of low and higher risk samples. Two groups were then used to train the LD model. The withheld group was then used as a test of the performance of the model. This process was then repeated two more times, holding out one of the other groups respectively.

3 | RESULTS AND DISCUSSION

Figure 3A shows the collagen abundance within the tumor regions. Despite a slightly higher mean in the higher risk samples ($\mu = 0.51$ and 0.61 respectively), the KS test did not indicate statistically significant separation between the risk groups. This is somewhat at odds with previous literature reports that show that the relative abundance of collagenous intratumoural stroma to be prognostically informative in breast cancer.^[14–19] However, many of these studies use small, tightly defined ROIs in locations subjectively deemed to be the most invasive pathology in the sample. It is likely that the large ROIs used in this study, with the intentional inclusion of intrasample heterogeneity, increased the variance of the populations and reduced the significance of their separation. The average cumulative tumor area analyzed per sample was 62.5mm^2 . For context, a review of TSR prognostication studies by Mesker et al^[17] reported ROIs of roughly 9mm^2 , and a recent analysis of collagen alignment in renal cell carcinoma used ROIs on the order of 1mm^2 .^[30] By avoiding ROIs based on a narrowly defined (and often subjective) selection criteria and by sampling a relatively large area per slide, we aimed to limit bias and generate more representative results inclusive of tumor heterogeneity; the potential downside of such large ROI selection in the increased variance in the results that may mask the low- vs higher risk OncotypeDx intergroup differences. Comparatively large ROIs were chosen for the purpose of minimizing subjectivity and operator bias.

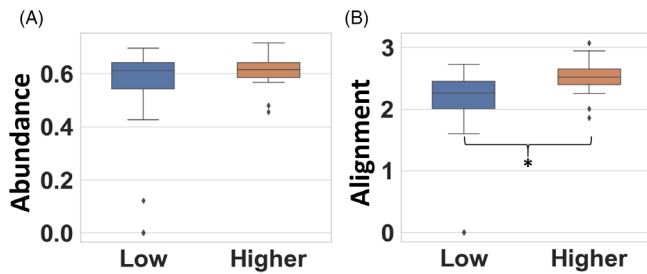


FIGURE 3 Boxplots showing the mean of the two different polarimetry-derived metrics of A, intratumoural collagen abundance ($\mu = 0.51$, $\sigma = 0.23$, median = 0.61 and $\mu = 0.61$, $\sigma = 0.06$, median = 0.61, respectively) and B, peri-tumoural collagen alignment ($\mu = 1.9$, $\sigma = 0.82$, median = 2.2 and $\mu = 2.5$, $\sigma = 0.31$, median = 2.5, respectively). * indicates a statistically significant difference ($P < .01$) using the two-sample KS test. For each box plot, the central line shows the median of the groups, the box denotes the second and third quartiles, the whiskers indicate the first and fourth quartile, respectively, and outliers are demarcated by symbols. Although some differences exist in the intratumoural collagen abundance (A), it is only in the alignment of peri-tumoural collagen that a statistically significant difference between the low and higher risk groups was noted (B). The outlier (with a value close to zero for both metrics) had a high amount of mucin surrounding the tumor with very little collagen present for our birefringence analysis. Color is indicative of risk group. KS, Kolmogorov–Smirnov

The involvement of a single pathologist at this stage seemed reasonable considering these large ROIs and the pathologist's relatively straight forward task (selecting and contouring tumor-cell rich areas). A final impetus for the proposed ROI selection criteria and size was to mitigate the possible confounding effects from structures of high organization but low-diagnostic power such as vessels or nerves. At this stage, such regions have not been excluded. These may indeed present a source of variability, for example, artificially increasing the alignment of mostly misaligned collagenous stroma. However, in addition to the intentional choice of large ROIs, we expect their effect to be relatively small for two reasons: (1) the stromal abundance is much higher compared to such vessels and nerves^[31]; (2) these are likely present across all samples (low or higher risk groups), so their impact on the group differentiation should be limited.

Figure 3B shows the collagen alignment in the leading edge for the low and higher risk groups. Here, the KS test did indicate statistically significant ($P < .01$) separation between the risk groups. A lower degree of collagen alignment in the higher risk samples is in line with previous tumor-collagen studies and has been shown to be indicative of more aggressive disease.^[11, 20–23] This is particularly encouraging in light of our efforts to objectively choose large ROIs to account for intrasample heterogeneity:

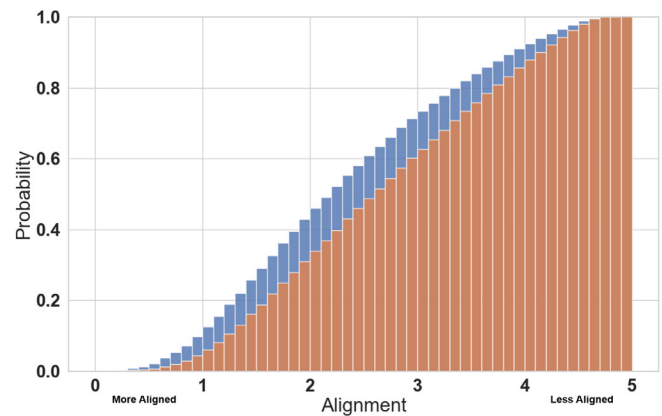


FIGURE 4 The aggregated CDFs for the alignment of the leading edge collagen for low (blue) and higher (orange) risk groups. Of note is the greater proportion of aligned collagen for the low-risk group. In subsequent analysis, the root mean squared error (RMSE) is calculated between each sample's CDF and the “population” CDFs of the two risk groups. CDF, cumulative density functions

despite the resultant increase in sample variance that this introduces, a significant separation between the two group was still demonstrated. A potential causal link between the OncotypeDx risk score and collagenous stroma morphology is found in the two “invasion” genes, stromelysin 3 and cathepsin L2, from the 21-gene panel that OncotypeDX considers. These genes promote the invasion of the tumor into the host tissue through a reorganization of the surrounding collagen.^[32] Stromelysin 3, a matrix metalloproteinase, is involved in the degradation of collagen and other constituents in the ECM and is often over-expressed in breast cancer.^[32, 33]

As mentioned in the methods section, the analysis of collagen alignment in the leading edge ROIs resulted in a distribution of values for each sample. The analysis summarized in Figure 3B collapsed these distributions into a single value (their mean) and compared the differences in the means between the risk groups. Although statistically significant results were obtained, there is more information in the actual distributions than can be captured in such single number representation. Figure 4 thus shows the aggregated CDFs for the two risk groups, demonstrating where the risk group distributions differ. Compared to the higher risk group, the low-risk group histogram is left shifted indicating a higher prevalence of aligned collagen. The maximum difference between the CDFs occurs at the median of the low-risk alignments (alignment metric = 2.26) and has a value of 0.126. Therefore, collagen in the leading edge of a low-risk sample has a 12.6% greater chance of being more aligned with its neighbors than collagen from the higher risk group.

The separation that occurs between the two CDFs in Figure 4 motivated their use in the effort to retrospectively classify a patient's sample as low or higher risk. As mentioned previously, incorporation of the entire 60 bins of the histogram as predictive features would result in a prohibitively high dimensionality of predictor variables. This challenge motivated the use of the RMSE between each sample and the two aggregate class histograms, as a way of retaining much of the separatory information that the distributions contained.

The position of the samples in the RMSE space is shown in Figure 5A. The vertical axis represents the difference between each sample's leading edge collagen alignment CDF and the combined low-risk CDF; similarly, the horizontal axis is the difference between each sample and the combined higher risk CDF. As expected, the higher risk samples (orange markers) tend to have larger values along the vertical axis (as their distributions are, on average, more different from the combined low-risk distributions). Analogously, the low-risk samples (blue markers) have larger values along the horizontal axis. This RMSE data served as input for the LD model training. Note that as 3-fold cross-validation was used during the computation of the LD model, only two thirds of this data were in use at a time (as the third group was held out to act as a test set). The line of separation between the classes, as found by the LD model, is represented by the dashed line in Figure 5A. Any sample that lies in the region above the line is classified as higher risk by the model, and those

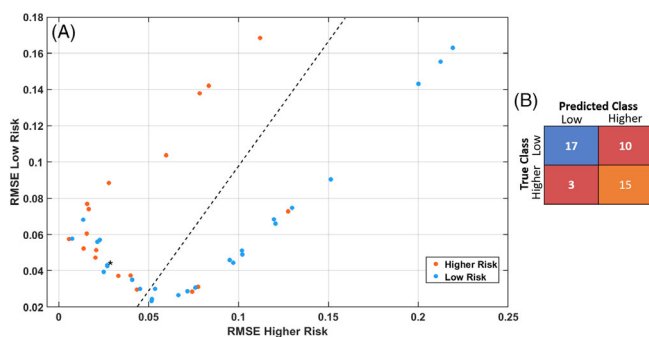


FIGURE 5 A, Scatter plot showing the RMSE of each sample relative to the low and higher risk aggregate CDFs. Each point represents a sample, and color indicates OncotypeDX risk group. The dotted line shows the separation boundary from the LD model. Samples that lie above it were classified as higher risk, samples below as low risk. B, Confusion matrix showing the number of correctly (diagonal, blue and orange) and incorrectly (off-diagonal, red) samples classified by the LD model (trained with an emphasis for higher risk sensitivity to correctly classify higher risk samples). While only achieving 71% total accuracy, the model exhibited 83% sensitivity to the higher risk group. Note that the marker with the asterisk represents three low-risk samples. CDF, cumulative density functions; LD, linear discriminant

below it are classified as low risk. Stemming from the significantly increased weight of misclassifications of higher risk samples as low risk, the model does not optimize total accuracy, but rather sensitivity to the higher risk samples. That is, the total overall classification accuracy was sacrificed in order to decrease the occurrence of false negatives in classifying higher risk samples (since such a “mistake” would be more clinically significant than misclassifying a low-risk sample as higher risk). Figure 5B summarizes the performance of the LD model in a confusion matrix. Although total accuracy (71%) is reduced due to modest low-risk accuracy classification (63%), a high sensitivity to the higher risk samples was achieved (83%). This is encouraging in approaching the ~10% false negative rate that is required in other breast cancer contexts such as sentinel lymph node assessment,^[34] and in light of the sensitivity and specificity of OncotypeDX to high-risk samples, ~93% and 30% respectively,^[5] using 10-year recurrence as the quantifiable endpoint.

Polarimetric imaging for collagen analysis has become quite widespread. Studies often involve an imaging methodology that fully characterizes the polarimetric properties of the tissue by the determination of the Mueller matrix.^[24] Technologically, Mueller polarimetry is more complex, and the results can be difficult to interpret. This is contrasted with the simpler rotating-crossed-linear-polarizers method and direct derivation of collagen metrics used here. Comparing the two techniques in terms of their resultant information content, Mueller approaches give a complete characterization of the tissue polarization properties at the expense of more complex methodology. The added value of this extra information depends on the task-specific application. For the assessment of collagenous stroma abundance and alignment, our imaging approach provides specific metrics that describe these features while allowing for simple, inexpensive and rapid methodology.

There have been several other studies probing the link between OncotypeDx risk scores and clinicopathologic or histopathologic features.^[35–37] These features often include Nottingham grade, tumor size, lobular or tubular subtypes, TSR and age, among others. The correlation of OncotypeDx risk score with these features have consistently shown reasonably accurate results (~70%–80% total accuracy). The LD model proposed here agrees quite well with these results, which is particularly encouraging given that this discriminatory power arose from only one feature, as opposed to the 7 to 12 features utilized in other studies^[35–37]; this suggests a potentially large source of previously untapped, polarimetrically obtainable, information about tumor behavior and prognosis. Future work will examine a larger clinical dataset and a broader array of polarimetric variables to build upon the promising results shown here.

4 | CONCLUSION

OncotypeDx is a powerful prognostic tool that has lent itself well to widespread clinical adoption. However, despite its overall integration into clinical workflows, there remain persistent problems with the technique.^[7–9] For example, several studies have remarked on the “black box” nature of the genetic test, as individual protein expression data is not made available.^[9] The cost of this test can also be prohibitive in resource-limited environments. As a result, further stratification of patient risk that can complement OncotypeDX would be clinically rewarding.

As a first step to such stratification, we have polarimetrically investigated the abundance of intratumoural collagen and the alignment of collagen in the leading edge and assessed their correlations with OncotypeDX risk group for a cohort of human IDC surgical samples. Using a novel form of PLM, collagen alignment in the leading edge was found to be significantly lower ($P < .01$) in higher OncotypeDX risk groups. Interestingly, no such difference was found for the collagen abundance from the tumor regions.

As mentioned above, previous studies have correlated OncotypeDx risk score with clinicopathological variables and shown reasonably accurate results in the separation of risk groups. In the present study, a LD model based on collagen alignment derived from PLM images has been shown to be 83% sensitive to low-risk groups, with an overall (albeit reduced) accuracy of 71%, comparing very well to these studies^[35–37] These results motivate future studies investigating using this novel PLM technique to study morphological changes within TME, and their correlation with clinically and scientifically important outcomes.

ACKNOWLEDGMENTS

The authors would like to thank James Jonkman and the staff at the Advanced Optical Microscopy Facility. This work was supported by the Canadian Institutes of Health Research (CIHR, PJT-156110) and the Natural Sciences and Engineering Research Council (NSERC, 410009540).

CONFLICT OF INTEREST

The authors declare no financial or commercial conflict of interest.

DATA AVAILABILITY STATEMENT

The data that support the findings of this study are available from the corresponding author upon reasonable request.

ORCID

Blake Jones  <https://orcid.org/0000-0002-6804-7521>

REFERENCES

- [1] F. Bray, J. Ferlay, I. Soerjomataram, R. L. Siegel, L. A. Torre, A. Jemal, *CA Cancer J. Clin.* **2018**, 68(6), 394.
- [2] K. Polyak, *J. Clin. Invest.* **2011**, 121(10), 3786.
- [3] S. Paik, G. Tang, S. Shak, C. Kim, J. Baker, W. Cronin, F. L. Baehner, D. Watson, J. Bryant, J. P. Costantino, C. E. Geyer Jr., D. L. Wickerham, N. Wolmark, *J. Clin. Oncol.* **2006**, 24(23), 3726.
- [4] K. S. Albain, W. E. Barlow, S. Shak, G. N. Hortobagyi, R. B. Livingston, I. T. Yeh, P. Ravdin, R. Bugarini, F. L. Baehner, N. E. Davidson, G. W. Sledge, E. P. Winer, C. Hudis, J. N. Ingle, E. A. Perez, K. I. Pritchard, L. Shepherd, J. R. Gralow, C. Yoshizawa, C. Allred, C. K. Osborne, D. F. Hayes, *Lancet Oncol.* **2010**, 11(1), 55.
- [5] J. A. Sparano, R. J. Gray, D. F. Makower, K. I. Pritchard, K. S. Albain, D. F. Hayes, C. E. Geyer Jr., E. C. Dees, M. P. Goetz, J. A. Olson, T. Lively, S. S. Badve, T. J. Saphner, L. I. Wagner, T. J. Whelan, M. J. Ellis, S. Paik, W. C. Wood, P. M. Ravdin, M. M. Keane, H. L. G. Moreno, P. S. Reddy, T. F. Goggins, I. A. Mayer, A. M. Brufsky, D. L. Toppmeyer, V. G. Kaklamani, J. L. Berenberg, J. Abrams, G. W. Sledge Jr., *N. Engl. J. Med.* **2018**, 379(2), 111.
- [6] M. B. Hannouf, G. S. Zaric, P. Blanchette, C. Brezden-Masley, M. Paulden, C. McCabe, J. Raphael, M. Brackstone, *Pharmacogenomics J.* **2019**, 1, 27.
- [7] C. B. Weldon, J. R. Trosman, W. J. Gradishar, A. B. Benson III, J. C. Schink, *J. Oncol. Pract.* **2012**, 8(4), e24.
- [8] R. Gyanchandani, Y. Lin, H. Lin, K. Cooper, D. P. Normolle, A. Brufsky, M. Fastuca, W. Crosson, S. Oesterreich, N. E. Davidson, R. Bhargava, D. J. Dabbs, A. V. Lee, *Clin. Cancer Res.* **2016**, 22(21), 5362.
- [9] V. Schildgen, M. Warm, M. Brockmann, O. Schildgen, *Sci. Rep.* **2019**, 9(1), 1.
- [10] D. J. Waterhouse, C. R. M. Fitzpatrick, B. W. Pogue, J. P. B. O'Connor, S. E. Bohndiek, *Nat. Biomed. Eng.* **2019**, 3(5), 339.
- [11] M. W. Conklin, P. J. Keely, *Cell Adh. Migr.* **2012**, 6(3), 249.
- [12] D. Hanahan, L. M. Coussens, *Cancer Cell* **2012**, 21(3), 309.
- [13] M. M. Mueller, N. E. Fusenig, *Nat. Rev. Cancer* **2004**, 4(11), 839.
- [14] C. L. Downey, S. A. Simpkins, J. White, D. L. Holliday, J. L. Jones, L. B. Jordan, J. Kulka, S. Pollock, S. S. Rajan, H. H. Thygesen, A. M. Hanby, V. Speirs, *Br. J. Cancer* **2014**, 110(7), 1744.
- [15] C. L. Downey, H. H. Thygesen, N. Sharma, A. M. Shaaban, *Springerplus* **2015**, 4(1), 68.
- [16] E. M. de Kruijf, J. G. H. van Nes, C. J. H. van de Velde, H. Putter, V. T. H. B. M. Smit, G. J. Liefers, P. J. K. Kuppen, R. A. E. M. Tollenaar, W. E. Mesker, *Breast Cancer Res. Treat.* **2011**, 125(3), 687.
- [17] C. J. H. Kramer, K. M. H. Vangangelt, G. W. van Pelt, T. J. A. Dekker, R. Tollenaar, W. E. Mesker, *Breast Cancer Res. Treat.* **2019**, 173(1), 55.
- [18] W. E. Mesker, J. M. C. Junggeburgt, K. Szuhai, P. de Heer, H. Morreau, H. J. Tanke, R. A. E. M. Tollenaar, *Anal. Cell. Pathol.* **2007**, 29(5), 387.
- [19] P. Aurello, G. Berardi, D. Giulitti, A. Palumbo, S. Maria Tierno, G. Nigri, F. D'Angelo, E. Pillozzi, G. Ramacciato, *Surgical* **2017**, 15(6), 329.
- [20] M. W. Conklin, J. C. Eickhoff, K. M. Riching, C. A. Pehlke, K. W. Eliceiri, P. P. Provenzano, A. Fried, P. J. Keely, *Am. J. Pathol.* **2011**, 178(3), 1221.

- [21] P. P. Provenzano, K. W. Eliceiri, J. M. Campbell, D. R. Inman, J. G. White, P. J. Keely, *BMC Med.* **2006**, *4*(1), 38.
- [22] J. S. Bredfeldt, Y. Liu, M. W. Conklin, P. J. Keely, T. R. Mackie, K. W. Eliceiri, *J. Pathol. Inform.* **2014**, *5*(1), 28.
- [23] Z.-H. Zhou, C.-D. Ji, H.-L. Xiao, H.-B. Zhao, Y.-H. Cui, X.-W. Bian, *J. Cancer* **2017**, *8*(8), 1466.
- [24] Y. Dong, J. Qi, H. He, C. He, S. Liu, J. Wu, D. S. Elson, H. Ma, *Biomed. Opt. Express* **2017**, *8*(8), 3643.
- [25] J. Westreich, M. Khorasani, B. Jones, V. Demidov, S. Nofech-Mozes, A. Vitkin, *Biomed. Opt. Express* **2019**, *10*(8), 3963.
- [26] B. Jones, G. Thomas, J. Westreich, S. Nofech-Mozes, A. Vitkin, M. Khorasani, *Biomed. Opt. Express* **2020**, *11*, 3246.
- [27] M. F. G. Wood, N. Vurgun, M. A. Wallenburg, I. A. Vitkin, *Phys. Med. Biol.* **2011**, *56*(8), N115.
- [28] K. Shen, S. Luk, D. F. Hicks, J. S. Elman, S. Bohr, Y. Iwamoto, R. Murray, K. Pena, F. Wang, E. Seker, R. Weissleder, M. L. Yarmush, M. Toner, D. Sgroi, B. Parekkadan, *Nat. Commun.* **2014**, *5*, 1.
- [29] A. Neesse, P. Michl, K. K. Frese, C. Feig, N. Cook, M. A. Jacobetz, M. P. Lolkema, M. Buchholz, K. P. Olive, T. M. Gress, D. A. Tuveson, *Gut* **2011**, *60*(6), 861.
- [30] S. L. Best, Y. Liu, A. Keikhosravi, C. R. Drifka, K. M. Woo, G. S. Mehta, M. Altwegg, T. N. Thimm, M. Houlihan, J. S. Bredfeldt, E. J. Abel, W. Huang, K. W. Eliceiri, *BMC Cancer* **2019**, *19*(1), 490.
- [31] P. Taroni, G. Quarto, A. Pifferi, F. Abbate, N. Balestreri, S. Menna, E. Cassano, R. Cubeddu, *PLoS One* **2015**, *10*(6), e0128941.
- [32] S. Paik, S. Shak, G. Tang, C. Kim, J. Baker, M. Cronin, F. L. Baehner, M. G. Walker, D. Watson, T. Park, W. Hiller, E. R. Fisher, D. L. Wickerham, J. Bryant, N. Wolmark, *N. Engl. J. Med.* **2004**, *351*(27), 2817.
- [33] N. Rouyer, C. Wolf, M. P. Chenard, M. C. Rio, P. Chambon, J. P. Bellocq, P. Basset, *Invasion Metastasis* **1994**, *14*(1–6), 269.
- [34] S. L. Wong, M. J. Edward, C. Chao, T. M. Tuttle, R. D. Noyes, D. J. Carlson, P. B. Cerrito, K. M. McMasters, *J. Am. Coll. Surg.* **2001**, *192*(6), 684.
- [35] M. B. Flanagan, D. J. Dabbs, A. M. Brufsky, S. Beriwal, R. Bhargava, *Mod. Pathol.* **2008**, *21*(10), 1255.
- [36] A. Orucevic, J. L. Bell, M. King, A. P. McNabb, R. E. Heidel, *The Breast* **2019**, *46*, 116.
- [37] J. Whitney, G. Corredor, A. Janowczyk, S. Ganesan, S. Doyle, J. Tomaszewski, M. Feldman, H. Gilmore, A. Madabhushi, *BMC Cancer* **2018**, *18*(1), 610.

How to cite this article: Jones B, Thomas G, Sprenger J, Nofech-Mozes S, Khorasani M, Vitkin A. Peri-tumoural stroma collagen organization of invasive ductal carcinoma assessed by polarized light microscopy differs between OncotypeDX risk group. *J. Biophotonics*. 2020;13: e202000188. <https://doi.org/10.1002/jbio.202000188>